proceedings

MDPI

Article

Influence of Spatial and Dynamical Anisotropies on Flow and Femtoscopy Radii in Relativistic Heavy-Ion Collisions at LHC Energies †

E. E. Zabrodin [1,2,*], L. V. Bravina [2], I. P. Lokhtin [1], L. V. Malinina [1,3], S. V. Petrushanko [1] and A. M. Snigirev [1]

1 Skobeltsyn Institute of Nuclear Physics, Moscow State University, RU-119991 Moscow, Russia; lokhtin@cern.ch (I.P.L.); ludmila.malinine@cern.ch (L.V.M.); Serguei.Petrouchanko@cern.ch (S.V.P.); Alexandre.Sniguirev@cern.ch (A.M.S.)

2 Department of Physics, University of Oslo, PB 1048 Blindern, N-0316 Oslo, Norway; larissa.bravina@fys.uio.no

3 Joint Institute for Nuclear Researches, RU-141980 Dubna, Russia

* Correspondence: eugen.zabrodin@fys.uio.no

† Presented at the 7th International Conference on New Frontiers in Physics (ICNFP 2018), Crete, Greece, 4–12 July 2018.

Published: 20 May 2019

Abstract: We study the influence of spatial and dynamical anisotropies in relativistic heavy-ion collisions on the differential elliptic and triangular flows of charged hadrons and, simultaneously, on the second- and third-order oscillations of the femtoscopic radii. Calculations of Pb + Pb collisions at $\sqrt{s} = 2.76$ TeV were done within the HYDrodynamics with JETs (HYDJET++) event generator, which allows one to investigate the role of each of the anisotropy kinds separately. It is found that the bare geometric anisotropy provides either the wrong sign of elliptic and triangular flows or out-of-phase oscillations of R^2_{out} and R^2_{side}, respectively. Dynamical anisotropy is able to describe qualitatively both characteristics correctly. For the correct quantitative description of the data, one has to employ both spatial and dynamical anisotropies.

Keywords: relativistic heavy-ion collisions; dynamical and spatial anisotropy; elliptic and triangular flow; azimuthal oscillations of femtoscopic radii

1. Introduction

Anisotropic flow of hadrons in relativistic heavy-ion collisions is a very convenient tool to probe the early stage of the collisions and to search for a new state of matter, quark-gluon plasma (QGP). To quantify the flow, the particle distribution in the azimuthal plane is decomposed in Fourier series [1]:

$$\frac{dN}{d\phi} \propto 1 + 2\sum_{n=1}^{\infty} v_n \cos\left[n(\phi - \Psi_n)\right], \quad (1)$$

with ϕ and Ψ_n being the azimuthal angle between the transverse momentum of a particle and the event plane and the azimuth of the event plane of the n^{th} component of the flow, respectively. The anisotropic flow components are identified as coefficients of the Fourier expansion:

$$v_n = \langle \cos\left[n(\phi - \Psi_n)\right] \rangle, \quad (2)$$

where one has to average over all particles in an event and over all event statistics. The first flow harmonics are called directed, v_1, elliptic, v_2, triangular, v_3, flow, and so on. The reasons causing

the formation of anisotropic flow in the system of colliding nuclei can be subdivided into the spatial, or geometric, anisotropies and the dynamical ones. In the first case, the spatial anisotropy ε_n of the overlapping zone of two nuclei is translated into the momentum anisotropy v_n during the expansion of the fireball. Note that only elliptic and triangular flows seem to be directly proportional to ε_2 and ε_3, respectively [2], mainly because of the non-linear contributions of the lower flow harmonics to the higher ones [3,4]. On the other hand, the non-isotropic azimuthal dependence of transverse velocity also causes the anisotropic flow even for spherically-symmetric sources [5]. This is an example of dynamical anisotropy. To check what kind of anisotropy, spatial or dynamical, dominates in relativistic heavy-ion collisions, one has to find another signal, which is influenced by both types of the anisotropy. The very good candidates for such a signal are azimuthal oscillations of femtoscopic radii in the Ψ_2 and Ψ_3 planes. Recall that in the femtoscopy analysis [6–8], the 3D correlation functions depend on the out, side, and long components of the relative momentum vector $\mathbf{q} = \{q_o, q_s, q_l\}$ [9–11] of a pair of particles and on the correlation radii R_o, R_s, R_l and their cross terms as:

$$CF(\mathrm{q}, \Phi) - 1 = \lambda \exp\left[-R_{\mathrm{o}}^2(\Phi) q_{\mathrm{o}}^2 - R_{\mathrm{s}}^2(\Phi) q_{\mathrm{s}}^2 - R_{\mathrm{l}}^2(\Phi) q_{\mathrm{l}}^2 - R_{\mathrm{o,s}}^2(\Phi) q_{\mathrm{o}} q_{\mathrm{s}} - R_{\mathrm{o,l}}^2(\Phi) q_{\mathrm{o}} q_{\mathrm{l}} - R_{\mathrm{s,l}}^2(\Phi) q_{\mathrm{s}} q_{\mathrm{l}}\right]. \quad (3)$$

Here, radii R_o, R_s, R_l indicate the sizes of the emitting source, λ is the so-called correlation strength, and Φ is the azimuthal angle of the pair momentum $\mathbf{q}$ with respect to the reaction plane. A sophisticated modern analysis considers bins of $\Delta\phi_n = \Phi - \Psi_n$ defined in the range $(0, \pi)$. The oscillations of femtoscopic radii w.r.t. the reaction planes of elliptic flow Ψ_2 and triangular flow Ψ_3 were found experimentally in heavy-ion collisions at energies of RHIC [12] and LHC [13,14]. For brevity, these oscillations are dubbed second-order and third-order oscillations, respectively. The investigation of interconnections between the femtoscopic oscillations and the source anisotropy was the subject of several papers; see, e.g., [15–19] and the references therein. The studies agree well that the third-order oscillations are mainly due to the dynamical anisotropy. The situation is not so obvious for the case of second-order oscillations. The early study [15] hints that these oscillations are determined by the spatial anisotropy, whereas recent investigations claim that both second-order and third-order oscillations are dominated by the dynamical anisotropy.

Our analysis employs the HYDrodynamics with JETs (HYDJET++) model. Its basic features are sketched in Section 2. Section 3 presents the main results of our study. Since HYDJET++ applies both sources of the anisotropy for the description of v_2 and v_3 and allows us to switch these sources on or off during the generation of events, it is very instructive to check the influence of mere spatial or dynamical anisotropy on the simultaneous description of the flow components and the oscillations of the femtoscopic radii. Conclusions are drawn in Section 4.

2. HYDJET++ Model

The abbreviation HYDJET++ means HYDrodynamics with JETs model, written in C++ [20]. The event generator consists of two parts responsible for the treatment of soft and hard processes, respectively. The soft block employs the adapted FASTMC event generator [5,21]. It assumes the sudden freeze-out scenario for the fireball at given temperature T and starts with the generation of the whole system on chemical and thermal freeze-out hypersurfaces. The latter are obtained from the parametrization of relativistic ideal hydrodynamics.

The block for description of hard processes relies on the jet quenching model PYQUEN [22]. Here, the collisional energy losses are calculated in the high-momentum transfer limit [23,24], and the radiative energy loss of a parton is estimated within the framework of the BDMS model [25–27]. The nuclear shadowing effect of parton distribution functions is obtained via the impact parameter-dependent parametrization [28] calculated within the Glauber–Gribov theory.

The generation of elliptic and triangular flows in HYDJET++ is organized as follows. The spatial elliptic modulation of the freeze-out hypersurface $\varepsilon_2(b)$ at given impact parameter b determines the transverse radius of the fireball:

$$R_{ell}(b,\phi) = R_f(b)\frac{\sqrt{1-\varepsilon_2^2(b)}}{\sqrt{1+\varepsilon_2(b)\cos 2\phi}}\,, \tag{4}$$

$$R_{\rm f}(b) = R_0\sqrt{1-\varepsilon_2(b)}\,, \tag{5}$$

where R_0 is the freeze-out transverse radius for the collision at the zero impact parameter. Since each of the fluid cells is carrying its own momentum, the spatial anisotropy of the source is transformed into the momentum anisotropy. Dynamical anisotropy is controlled by the momentum flow anisotropy parameter $\delta_2(b)$, which links the azimuthal angle of the fluid cell velocity ϕ_{cell} to the azimuthal angle ϕ via the relation:

$$\tan\phi_{cell} = \tan\phi\sqrt{\frac{1-\delta_2(b)}{1+\delta_2(b)}}\,. \tag{6}$$

Note that if $\delta_2 \neq 0$, even the spherically-symmetric source would develop non-zero elliptic flow [5]. The parameter ε_2 implicitly regulates the modulation magnitude of the radial velocity via its dependence on a radial position of the fluid cell, whereas the parameter δ_2 determines the non-zero value of the tangential velocity and also influences the modulation magnitude of the transverse velocity. The alternative approach implies the direct dynamical modification of the radial flow only without changing the expansion direction of the fluid cell, $\phi_{cell} = \phi$. This option is also implemented in our Monte Carlo generator; see [20]. After comparison with the experimental data, it appears, however, that the latter parametrization poorly describes the momentum and centrality dependencies of elliptic flow, although it provides the correct qualitative behavior of the flow and the femtoscopy observables simultaneously.

Triangular flow in the model also depends on spatial and dynamical anisotropy parameters. It is worth mentioning that according to experimental data, the event plane of the triangular flow is randomly oriented in HYDJET++ w.r.t. the event plane of the elliptic flow. The modified radius reads:

$$R_{tr}(b,\phi) = R_{ell}(b)[1+\varepsilon_3(b)\cos[3(\phi-\Psi_3)]]\,, \tag{7}$$

where $\varepsilon_3(b)$ is the spatial triangularity of the fireball. Triangular dynamical anisotropy $\rho_3(b)$ leads to triangular modulation of the velocity profile:

$$\rho_{\rm u}^{max}(b) = \rho_{\rm u}^{max}(0)\,\{1+\rho_3(b)\cos[3(\phi-\Psi_3)]+\ldots\}\,, \tag{8}$$

with u being the four-velocity of the fluid cell. The attractive feature of HYDJET++ is that one can pick up just one of the key parameters, $\varepsilon_2, \varepsilon_3, \delta_2$, or ρ_3, whereas others are set to zero, and investigate the influence of the particular anisotropy on the flow components and femtoscopic radii. Another feature of the model is the rich table of resonances including the charmed ones. The model was further upgraded to event-by-event (EbyE) fluctuations of the flow harmonics [29]. Its further details can be found in [20]. Besides the EbyE fluctuations, HYDJET++ has been successfully tested for the description of both elliptic [30,31] and triangular [32,33] flows, higher flow harmonics [4,34,35], azimuthal di-hadron correlations [36], and the flow of mesons with hidden and open charm [37] in ultra-relativistic heavy ion collisions at energies of RHIC and LHC.

3. Results of the Simultaneous Description of v_2, v_3, and Oscillations of Femtoscopic Radii

In what follows, the Pb + Pb collisions at $\sqrt{s} = 2.76$ TeV are considered. Let us summarize briefly the experimental observations concerning elliptic and triangular flows and oscillations of femtoscopic radii. Differential elliptic flow of charged particles, $v_2^{ch}(p_T)$, is positive at $p_T \geq 0.1$ GeV/c. It increases with rising transverse momentum. Distribution $R^2_{side}(\Delta\phi_2)$, $\Delta\phi_2 = \phi_{pair} - \Psi_2$ reaches the maximum at $\Delta\phi_2 \approx \pi/2$, whereas $R^2_{out}(\Delta\phi_2)$ has the minimum there. The last distribution, $R^2_{long}(\Delta\phi_2)$, seems to have no distinct oscillations [13]. Differential triangular flow of charged particles, $v_3^{ch}(p_T)$, is also

positive and increasing with rising p_T. Both $R^2_{side}(\Delta\phi_3)$, $\Delta\phi_3 = \phi_{pair} - \Psi_3$ and $R^2_{out}(\Delta\phi_3)$ have maxima at $\Delta\phi_3 = \pi/3$, whereas $R^2_{long}(\Delta\phi_3)$ demonstrates no pronounced oscillations [14].

The convenient practical feature of the HYDJET++ model is that it permits one to switch off all but one parameter responsible for the flow anisotropy in order to study the influence of this particular factor on the development of flow and femtoscopic radii. The same is true for calculations with and without decays of resonances. The plan of our study is as follows. Having a set of four parameters, i.e., $\{\varepsilon_2, \delta_2, \varepsilon_3, \rho_3\}$, we are generating about two million lead-lead collisions with centrality $20\% \leq \sigma/\sigma_{geo} \leq 30\%$ at $\sqrt{s} = 2.76$ TeV with only one non-zero parameter, which can be positive or negative. Eight cases will be investigated, namely $\{\pm 0.3, 0, 0, 0\}$, $\{0, \pm 0.3, 0, 0\}$, $\{0, 0, \pm 0.3, 0\}$, and $\{0, 0, 0, \pm 0.3\}$. Note, that the listed values are almost an order of magnitude stronger than those employed usually for the description of the data. Our primary goal is to study the qualitative correspondence of model results, such as the sign of the differential flow and the positions of the oscillation extrema of femtoscopic radii, if any, to the experimental observations.

We start from the investigation of the role of elliptic anisotropy parameters. Firstly, only spatial anisotropy is left. The calculations with $\varepsilon_2 = \pm 0.3$ are displayed in Figure 1. ALICE data from [13] for the momentum interval $0.5 < k_T < 0.7$ GeV/c are plotted onto the calculations also. Recall that the main goal of our present study is the search for the influence of pure spatial and pure dynamical anisotropies on the harmonics of anisotropic flow and femtoscopic radii. Direct comparison of the model results and the data demands at least (i) an increase of the generated statistics by an order of magnitude, because the data are measured in much narrower k_T intervals ranging from 0.2 GeV/c–0.7 GeV/c, and (ii) application of both spatial and dynamical types of the anisotropy together with the fine-tuning of the anisotropy parameters. This research is out of the scope of our present investigation. Therefore, experimental data shown in Figure 1 and in other figures below are for qualitative comparison only. Experiments show that the oscillation phases of the femtoscopic radii are similar for all measured k_T intervals, whereas the source radii, $R_{out}, R_{side}, R_{long}$, increase with the diminishing of the k_T value. For a positive value of ε_2, both $R^2_{side}(\Delta\phi_2)$ and $R^2_{out}(\Delta\phi_2)$ of directly-produced particles have a maximum and a minimum, respectively, at $\Delta\phi \approx \pi/2$. Resonance decays, as was shown in [19], significantly increase the femtoscopic radii, but do not shift the phases of the oscillations. $R^2_{long}(\Delta\phi_2)$ seems to have a weak minimum at $\Delta\phi \approx \pi/2$. This qualitatively agrees with the data; however, the differential elliptic flow appears to be negative within the whole interval $0 \leq p_T \leq 3$ GeV/c, which is definitely wrong. In contrast, for the negative value of ε_2, the differential elliptic flow of charged hadrons becomes positive. However, in this case, both $R^2_{out}(\Delta\phi_2)$ and $R^2_{side}(\Delta\phi_2)$ oscillations are out-of-phase compared to the experimental distributions.

Next, we consider the non-zero dynamical elliptic anisotropy only, $\delta_2 = \pm 0.3$; see Figure 2. A positive value of δ_2 results in positive elliptic flow $v_2^{ch}(p_T)$. Furthermore, $R^2_{out}(\Delta\phi_2)$ has a maximum at $\Delta\phi_2 \approx \pi/2$, whereas $R^2_{side}(\Delta\phi_2)$ reaches here a local minimum, in accord with the data. Distributions obtained for the calculations with negative δ_2 provide us negative differential elliptic flow of hadrons and out-of-phase oscillations of $R^2_{side(out)}(\Delta\phi_2)$. Thus, we may conclude that in contrast to the earlier statement in [15], dynamical anisotropy dominates over the geometric one in the simultaneous description of elliptic flow and azimuthal oscillations of femtoscopic radii. As in the case with only the spatial anisotropy, decays of resonances increase the radii, but do not change the phases of the oscillations.

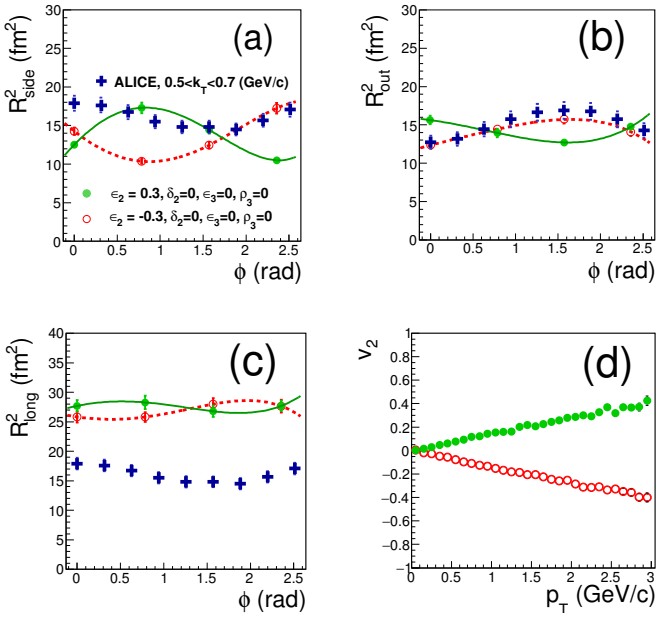

Figure 1. (**a**–**c**) The azimuthal dependence of $R^2_{side}(\Delta\phi_2)$, $R^2_{out}(\Delta\phi_2)$, and $R^2_{long}(\Delta\phi_2)$, respectively, in the HYDrodynamics with JETs (HYDJET++) calculations of Pb + Pb collisions at $\sqrt{s} = 2.76$ GeV with the centrality 20–30%. The k_T range is 0.2–2.0 GeV/c. (**d**) The differential elliptic flow of charged hadrons as a function of p_T. The distributions show calculations with $\varepsilon_2 = 0.3$ (solid circles) and with $\varepsilon_2 = -0.3$ (open circles). ALICE data from [13] for $0.5 < k_T < 0.7$ GeV/c are shown by crosses. Lines are drawn to guide the eye.

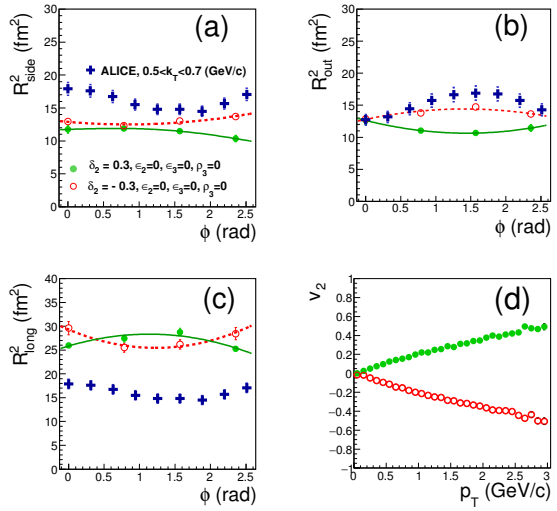

Figure 2. The same as Figure 1, but for calculations with $\delta_2 = 0.3$ (solid circles) and with $\delta_2 = -0.3$ (open circles).

Now, we turn to study the triangular anisotropy. All parameters except ε_3, responsible for spatial triangularity, are set to zero. Results of the calculations with $\varepsilon_3 = \pm 0.3$ are shown in Figure 3. Similarly to the study of elliptic anisotropy, for calculations of R^2_{out}, R^2_{long}, R^2_{side}, we plot the distributions for directly-produced particles only and for all hadrons after the decays of resonances. For a positive value of the spatial triangularity, $R^2_{side}(\Delta\phi_3)$ demonstrates a maximum at $\Delta\phi_3 \approx 0.75$ *rad* and a smeared minimum at $\Delta\phi_3 \approx 1.75$ *rad*. Distribution $R^2_{out}(\Delta\phi_3)$ has a minimum at $\Delta\phi_3 \approx 1.3$ *rad*, and a $R^2_{long}(\Delta\phi_3)$ has very weak maximum at $\Delta\phi_3 \approx 0.75$ *rad* and a minimum at $\Delta\phi_3 \approx 1.75$ *rad*, although a linear fit is still possible. Decays of resonances increase the absolute values of all three radii and make the the

oscillations more pronounced. However, they do not shift the extrema positions, i.e., no phase shift at all. This behavior is in line with the experimental observations [14] but unfortunately, the differential triangular flow $v_3^{ch}(p_T)$ is negative at $0 \leq p_T \leq 3$ GeV/c; see Figure 3d. The last result is obviously wrong. In contrast, calculations with negative spatial triangularity, $\varepsilon_3 = -0.3$, provide positive values for $v_3(p_T)$ and completely out-of-phase third-order oscillations of the femtoscopic radii squared. Again, as in the case of bare elliptic spatial anisotropy, one cannot describe correctly the qualitative behavior of both triangular flow and femtoscopic radii. The situation improves if one considers the non-zero dynamical anisotropy parameter, $\rho_3 = \pm 0.3$. Distributions corresponding to this case are depicted in Figure 4. Although the magnitudes of the oscillations are relatively weak, calculations with positive ρ_3 reproduce qualitatively the experimental results. Decays of resonances do not change the oscillation phases. Calculations with a negative dynamical anisotropy parameter contradict the data for both $v_3(p_T)$ and $R^2_{out,side,long}(\Delta\phi_3)$. Note also that for a quantitative description of the radii oscillations, we have to employ both spatial and dynamical anisotropy. One can see, however, that the relative magnitude of the radii oscillations is reproduced fairly well. For instance, ΔR^2_{out} and ΔR^2_{side} between the maxima and minima values do not exceed 15–20% for second-order oscillations [13] and 8–12% for third-order ones [14]. HYDJET++ calculations nicely match these results.

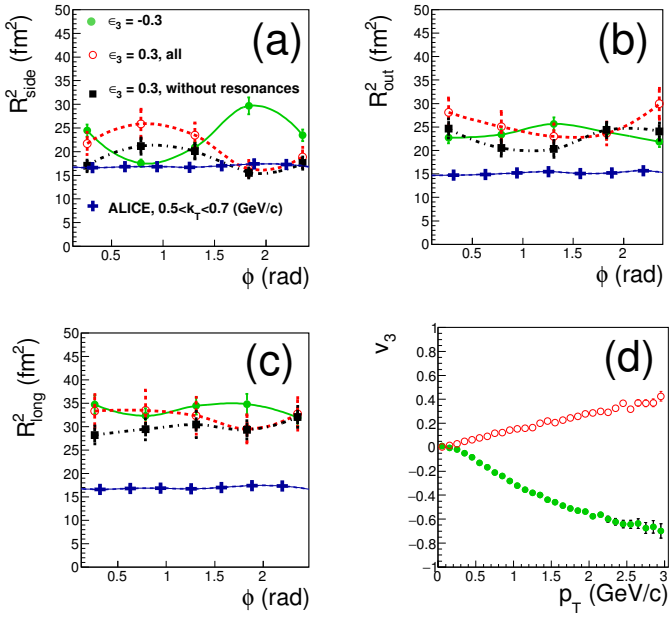

Figure 3. (**a**–**c**) The azimuthal dependence of $R^2_{side}(\Delta\phi_3)$, $R^2_{out}(\Delta\phi_3)$, and $R^2_{long}(\Delta\phi_3)$, respectively, in HYDJET++ calculations of Pb + Pb collisions at $\sqrt{s} = 2.76$ GeV with the centrality 20–30%. The k_T range is 0.2–2.0 GeV/c. (**d**) The differential triangular flow of charged hadrons as a function of p_T. The distributions show calculations with $\varepsilon_3 = 0.3$ (solid circles) and with $\varepsilon_3 = -0.3$ (open circles). Crosses denote the ALICE data for $0.5 < k_T < 0.7$ GeV/c from [14]. Lines are drawn to guide the eye.

Finally, we investigated the profiles of pion emission densities in the transverse plane for the separated cases of dynamical and spatial anisotropies. To make the results more distinct, we opted for the following values of the anisotropy parameters in HYDJET++: $\varepsilon_2 = 0.5$ or $\delta_2 = -0.3$ for the elliptic anisotropy and $\varepsilon_3 = 0.3$ or $\rho_3 = 0.5$ for the triangular anisotropy, respectively. Because pion emission densities depend strongly on the emission angles, the selected angular areas are (1) $0 < \phi \leq \pi/4$, (2) $\pi/4 < \phi \leq \pi/2$, and (3) $\pi/2 < \phi \leq 3\pi/4$ for the elliptic anisotropy, and (1′) $0 < \phi \leq \pi/6$, (2′) $\pi/3 < \phi \leq \pi/2$, and (3′) $2\pi/3 < \phi \leq 5\pi/6$ for the triangular anisotropy. HYDJET++ results for the elliptic anisotropy are displayed in Figure 5 for the cases of bare spatial and bare dynamical anisotropy, respectively. We see that the same-density contours of pion emission are sharper for spatial anisotropy compared to the dynamical one. Spatial anisotropy demonstrates also a stronger difference between

the emission zones at three different angles, thus explaining the stronger azimuthal dependence of $R^2_{side}(\Delta\phi_2)$ and $R^2_{out}(\Delta\phi_2)$, which is seen in Figure 1. Nevertheless, for both cases, the emitting areas have non-Gaussian shapes.

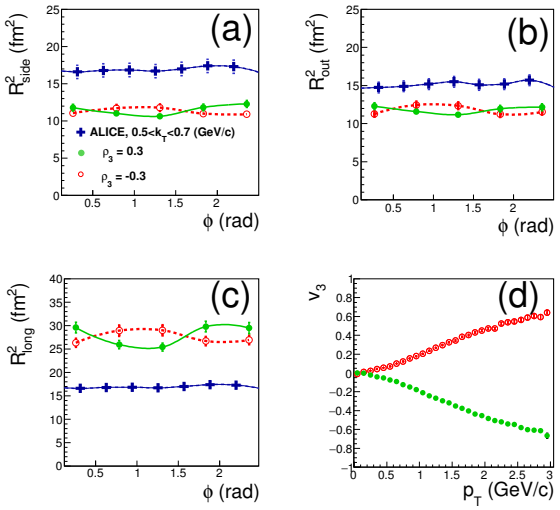

Figure 4. The same as Figure 3, but for calculations with $\rho_3 = 0.3$ (solid circles) and with $\rho_3 = -0.3$ (open circles).

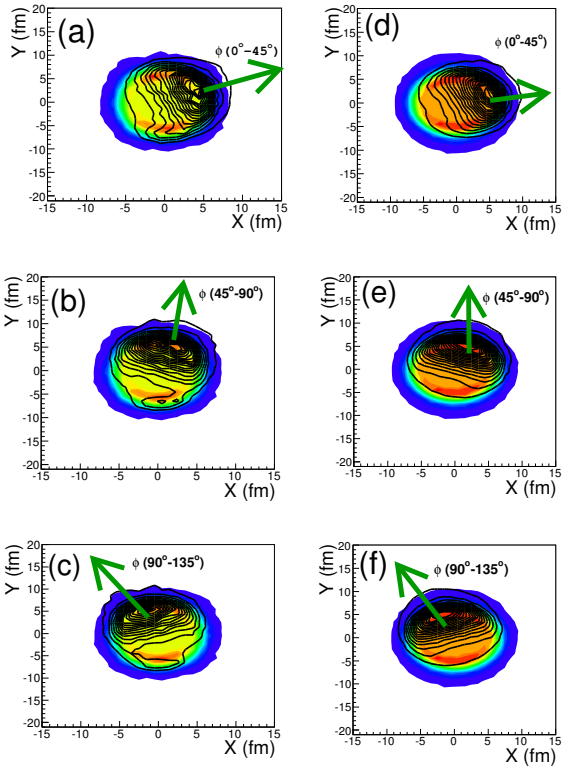

Figure 5. Pion emission function in the transverse plane of HYDJET++ simulated Pb + Pb collisions at $\sqrt{s} = 2.76$ TeV with centrality 20–30%. The left column displays calculations with only spatial elliptic anisotropy $\varepsilon_2 = 0.5$, whereas the right column presents results for non-zero dynamical anisotropy $\delta_2 = -0.3$. Shaded contours are identical for each column and indicate the density of emitted pions. Contour lines show the densities of pions emitted at angles $0 < \phi \leq \pi/4$ (**upper row**), $\pi/4 < \phi \leq \pi/2$ (**middle row**), and $\pi/2 < \phi \leq 3\pi/4$ (**bottom row**), respectively.

Calculations with non-zero triangular anisotropy parameters are shown in Figure 6. Similarly to Figure 5, here, the left figures present the results for spatial anisotropy, whereas the right figures show the influence of dynamical anisotropy only. Again, the difference for the emitting zones in three angular directions is stronger for the geometric anisotropy. The contours of pion densities are far from the Gaussians. The last circumstance seriously complicates the restoration of source's sizes and shapes by the standard methods of femtoscopic analysis.

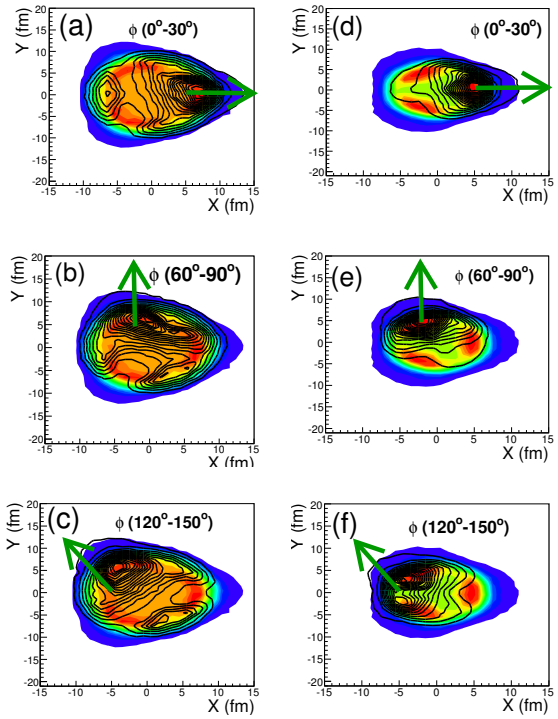

Figure 6. The same as Figure 5, but for calculations with non-zero geometric triangular anisotropy $\varepsilon_3 = 0.3$ (**left column**) and with non-zero dynamical triangular anisotropy $\rho_3 = 0.5$ (**right column**). Contour lines show the densities of pions emitted at angles $0 < \phi \leq \pi/6$ (**upper row**), $\pi/3 < \phi \leq \pi/2$ (**middle row**), and $2\pi/3 < \phi \leq 5\pi/6$ (**bottom row**), respectively.

4. Conclusions

We studied second- and third-order oscillations of the femtoscopic radii together the differential elliptic and triangular flow of charged particles in Pb + Pb collisions at $\sqrt{s} = 2.76$ TeV within the HYDJET++ model. The model has a set of parameters responsible for geometric and dynamical ellipticity and triangularity in the colliding system. It provides the opportunity to study the role of each of the anisotropy types separately. Our investigation reveals that the bare spatial anisotropy cannot describe simultaneously the oscillations of the femtoscopic radii in both the Ψ_2 and Ψ_3 planes and the correct sign of differential elliptic and triangular flows. Dynamical anisotropy qualitatively reproduces both signals; however, to match the experimental data quantitatively, one has to employ both sources of the anisotropy. Decays of resonances significantly increase the emitting areas in both planes of elliptic and triangular flow. Furthermore, these decays make the radii oscillations more pronounced, but they do not change the phases of the oscillations. Our results agree well with the findings of other models [16,18]. The shapes of the emission areas of pions are found to be far from the Gaussians, applied by default in standard femtoscopy analysis.

Author Contributions: All authors contributed equally to this work.

Funding: This work was supported by the Russian Foundation for Basic Research (RFBR) under grant No. 18-02-00155.

Acknowledgments: Fruitful discussions with E. Boos, L. Csernai, and R. Lednicky are gratefully acknowledged.

Conflicts of Interest: The authors declare no conflict of interests.

References

1. Voloshin, S.A.; Poskanzer, A.M.; Snellings, R. Collective phenomena in non-central nuclear collisions. *Landolt-Börnstein* **2010**, *23*, 293–333, doi:10.1007/978-3-642-01539-7_10.
2. Qin, G.-Y.; Petersen, H.; Bass, S.A.; Muller, B. Translation of collision geometry fluctuations into momentum anisotropies in relativistic heavy-ion collisions. *Phys. Rev. C* **2010**, *82*, 064903; doi:10.1103/PhysRevC.82.064903.
3. Borghini, N.; Ollitrault, J.-Y. Momentum spectra, anisotropic flow, and ideal fluids. *Phys. Lett. B* **2006**, *642*, 49–54, doi:10.1016/j.physletb.2005.08.131.
4. Bravina, L.V.; Brusheim Johansson, B.H.; Eyyubova, G.K.; Korotkikh, V.L.; Lokhtin, I.P.; Malinina, L.V.; Petrushanko, S.V.; Snigirev, A.M.; Zabrodin, E.E. Hexagonal flow v6 as a superposition of elliptic v2 and triangular v3 flows. *Phys. Rev. C* **2014**, *89*, 024909, doi:10.1103/PhysRevC.89.024909.
5. Amelin, N.S.; Lednicky, R.; Lokhtin, I.P.; Malinina, L.V.; Snigirev, A.M.; Karpenko, I.A.; Sinyukov, Y.M.; Arsene, I.; Bravina, L. Fast hadron freeze-out generator. Part II. Noncentral collisions. *Phys. Rev. C* **2008**, *77*, 014903, doi:10.1103/PhysRevC.77.014903.
6. Podgoretsky, M.I. Interference Correlations of Identical Pions: Theory (In Russian). *Fiz. Elem. Chast. Atom. Yadra* **1989**, *20*, 628–668.
7. Lednicky, R. Correlation femtoscopy of multiparticle processes. *Phys. Atom. Nucl.* **2004**, *67*, 72–82, doi:10.1134/1.1644010.
8. Lisa, M.; Pratt, S.; Soltz, R.; Wiedemann, U. Femtoscopy in relativistic heavy ion collisions. *Ann. Rev. Nucl. Part Sci.* **2005**, *55*, 357–402, doi:10.1146/annurev.nucl.55.090704.151533.
9. Podgoretsky, M.I. On the Comparison of Identical Pion Correlations in Different Reference Frames. *Sov. J. Nucl. Phys.* **1983**, *37*, 272–278.
10. Bertsch, G.F.; Danielewicz, P.; Herrmann, M. Hanbury-Brown-Twiss analysis in a solvable model. *Phys. Rev. C* **1994**, *49*, 442–451, doi:10.1103/PhysRevC.49.442.
11. Chapman, S.; Scotto, P.; Heinz, U. A New cross term in the two particle HBT correlation function. *Phys. Rev. Lett.* **1995**, *74*, 4400–4403, doi:10.1103/PhysRevLett.74.4400.
12. Niida, T. et al. [PHENIX Collaboration] Detailed HBT measurements with respect to the event plane and collision energy in Au+Au collisions at PHENIX. *Nucl. Phys. A* **2013**, *904*, 439c–442c, doi:10.1016/j.nuclphysa.2013.02.043.
13. Adamova, D.; et al. [ALICE Collaboration] Azimuthally Differential Pion Femtoscopy in Pb-Pb Collisions at $\sqrt{s_{NN}} = 2.76$ TeV. *Phys. Rev. Lett.* **2017**, *118*, 222301, doi:10.1103/PhysRevLett.118.222301.
14. Acharya, S.; et al. [ALICE Collaboration] Azimuthally-differential pion femtoscopy relative to the third harmonic event plane in Pb-Pb collisions at $\sqrt{s_{NN}} = 2.76$ TeV. *Phys. Lett. B* **2018**, *785*, 320–331, doi:10.1016/j.physletb.2018.06.042.
15. Heinz, U.; Kolb, P.F. Emission angle dependent pion interferometry at RHIC and beyond. *Phys. Lett. B* **2002**, *542*, 216–222, doi:10.1016/S0370-2693(02)02372-9.
16. Plumberg, C.J.; Shen, C.; Heinz, U. Hanbury-Brown–Twiss interferometry relative to the triangular flow plane in heavy-ion collisions. *Phys. Rev. C* **2013**, *88*, 044914, doi:10.1103/PhysRevC.88.044914.
17. Lökös, S.; Csanad, M.; Tomasik, B.; Csorgo, T. Higher order anisotropies in the Buda-Lund model: Disentangling flow and density field anisotropies. *Eur. Phys. J. A* **2016**, *52*, 311, doi:10.1140/epja/i2016-16311-y.
18. Cimerman, J.; Tomasik, B.; Csanad, M.; Lökös, S. Higher-order anisotropies in the Blast-Wave Model–Disentangling flow and density field anisotropies. *Eur. Phys. J. A* **2017**, *53*, 161, doi:10.1140/epja/i2017-12349-7.
19. Bravina, L.V.; Lokhtin, I.P.; Malinina, L.V.; Petrushanko, S.V.; Snigirev, A.M.; Zabrodin, E.E. Dynamical vs. geometric anisotropy in relativistic heavy-ion collisions. Which one prevails? *Eur. Phys. J. A* **2017**, *53*, 219, doi:10.1140/epja/i2017-12420-5.

20. Lokhtin, I.P.; Malinina, L.V.; Petrushanko, S.V.; Snigirev, A.M.; Arsene, I.; Tywoniuk, K. Heavy ion event generator HYDJET++ (HYDrodynamics plus JETs). *Comput. Phys. Commun.* **2009**, *180*, 779–799, doi:10.1016/j.cpc.2008.11.015.
21. Amelin, N.S.; Lednicky, R.; Pocheptsov, T.A.; Lokhtin, I.P.; Malinina, L.V.; Snigirev, A.M.; Karpenko, I.A.; Sinyukov, Y.M. A fast hadron freeze-out generator. *Phys. Rev. C* **2006**, *74*, 064901, doi:10.1103/PhysRevC.74.064901.
22. Lokhtin, I.P.; Snigirev, A.M. A Model of jet quenching in ultrarelativistic heavy ion collisions and high-p(T) hadron spectra at RHIC. *Eur. Phys. J. C* **2005**, *45*, 211–217, doi:10.1140/epjc/s2005-02426-3.
23. Braaten, E.; Thoma, M. Energy loss of a heavy fermion in a hot plasma. *Phys. Rev. D* **1991**, *44*, 1298–1310; doi:10.1103/PhysRevD.44.1298.
24. Lokhtin, I.P.; Snigirev, A.M. Nuclear geometry of jet quenching. *Eur. Phys. J. C* **2000**, *16*, 527–536, doi:10.1007/s100520000437.
25. Baier, R.; Dokshitzer, Y.L.; Mueller, A.H.; Peigne, S.; Schiff, D. Radiative energy loss of high-energy quarks and gluons in a finite volume quark-gluon plasma. *Nucl. Phys. B* **1997**, *483*, 291–320, doi:10.1016/S0550-3213(96)00553-6.
26. Baier, R.; Dokshitzer, Y.L.; Mueller, A.H.; Schiff, D. Angular dependence of the radiative gluon spectrum and the energy loss of hard jets in QCD media. *Phys. Rev. C* **1999**, *60*, 064902, doi:10.1103/PhysRevC.60.064902.
27. Baier, R.; Dokshitzer, Y.L.; Mueller, A.H.; Schiff, D. On the angular dependence of the radiative gluon spectrum. *Phys. Rev. C* **2001**, *64*, 057902, doi:DOI: 10.1103/PhysRevC.64.057902.
28. Tywoniuk, K.; Arsene, I.C.; Bravina, L.; Kaidalov, A.B.; Zabrodin, E. Gluon shadowing in the Glauber-Gribov model at HERA. *Phys. Lett. B* **2007**, *657*, 170–175, doi:10.1016/j.physletb.2007.09.065.
29. Bravina, L.V.; Fotina, E.S.; Korotkikh, V.L.; Lokhtin, I.P.; Malinina, L.V.; Nazarova, E.N.; Petrushanko, S.V.; Snigirev, A.M.; Zabrodin, E.E. Anisotropic flow fluctuations in hydro-inspired freeze-out model for relativistic heavy ion collisions. *Eur. Phys. J. C* **2015**, *75*, 588, doi:10.1140/epjc/s10052-015-3815-9.
30. Eyyubova, G.; Bravina, L.; Korotkih, V.L.; Lokhtin, I.P.; Malinina, L.V.; Petrushanko, S.V.; Snigirev, A.M.; Zabrodin, E. Jets and decays of resonances: Two mechanisms responsible for reduction of elliptic flow at the CERN Large Hadron Collider (LHC) and restoration of constituent quark scaling. *Phys. Rev. C* **2009**, *80*, 064907, doi:10.1103/PhysRevC.80.064907.
31. Zabrodin, E.E.; Bravina, L.V.; Eyyubova, G.K.; Lokhtin, I.P.; Malinina, L.V.; Petrushanko, S.V.; Snigirev, A.M. Influence of jets and resonance decays on the constituent quark scaling of elliptic flow. *J. Phys. G* **2010**, *37*, 094060, doi:10.1088/0954-3899/37/9/094060.
32. Crkovská, J.; Bielčík, J.; Bravina, L.; Johansson, B.H.B.; Zabrodin, E.; Eyyubova, G.; Korotkikh, V.L.; Lokhtin, I.P.; Malinina, L.V.; Petrushanko, S.V.; et al. Influence Jets Decays Reson. Triangular Flow Ultrarelativistic Heavy-Ion Collisions. *Phys. Rev. C* **2017**, *95*, 014910, doi:10.1103/PhysRevC.95.014910.
33. Zabrodin, E.E.; Bravina, L.V.; Brusheim Johansson, B.H.; Crkovská, J.; Eyyubova,G.K.; Korotkikh,V.L.; Lokhtin, I.P.; Malinina,L.V.; Petrushanko, S.V.; Snigirev, A.M. Features of triangular flow of strange and non-strange hadrons at LHC. *J. Phys. Conf. Ser.* **2016**, *668*, 012099, doi:10.1088/1742-6596/668/1/012099.
34. Bravina, L.V.; Brusheim Johansson, B.H.; Eyyubova, G.K.; Korotkikh, V.L.; Lokhtin, I.P.; Malinina, L.V.; Petrushanko, S.V.; Snigirev, A.M.; Zabrodin, E.E. Higher harmonics of azimuthal anisotropy in relativistic heavy ion collisions in HYDJET++ model. *Eur. Phys. J. C* **2014**, *74*, 2807, doi:10.1140/epjc/s10052-014-2807-5.
35. Bravina, L.; Brusheim Johansson, B.H.; Eyyubova, G.; Zabrodin, E. Effect of jets on the v_4/v_2^2 ratio, and constituent quark scaling in relativistic heavy-ion collisions. *Phys. Rev. C* **2013**, *87*, 034901, doi:10.1103/PhysRevC.87.034901.
36. Eyyubova, G.K.; Korotkikh, V.L.; Lokhtin, I.P.; Petrushanko, S.V.; Snigirev, A.M.; Bravina, L.V.; Zabrodin, E.E. Angular dihadron correlations as an interplay between elliptic and triangular flows. *Phys. Rev. C* **2015**, *91*, 064907, doi:10.1103/PhysRevC.91.064907
37. Lokhtin, I.P.; Belyaev, A.V.; Ponimatkin, G.; Pronina, E.Y.; Eyyubova, G.K. On the possibility of thermalization of heavy mesons in ultrarelativistic nuclear collisions. *J. Exp. Theor. Phys.* **2017**, *124*, 244–250, doi:10.1134/S1063776117010149.

© 2019 by the authors. Licensee MDPI, Basel, Switzerland. This article is an open access article distributed under the terms and conditions of the Creative Commons Attribution (CC BY) license (http://creativecommons.org/licenses/by/4.0/).